THERMOPHYSICAL PROPERTIES OF MERCURY: REVISITING MARINER 10 IRR MEASUREMENTS. J. L. Bandfield[1], M. M. Osterloo[2], and G. M. Holsclaw[2] [1]Space Science Institute (jbandfield@space-science.org), [2]Laboratory for Atmospheric and Space Physics, University of Colorado.

Introduction: The Mariner 10 Infrared Radiometer (IRR) collected a low latitude transect of ~11 and 45 μm radiance data across the night side Mercury in 1974. These data provided an initial determination of the thermophysical properties of the mercurian surface, including determination of a low thermal inertia regolith, similar to Earth's Moon [1]. Since Mariner 10 IRR, updated thermal models have been used to predict surface temperatures on Mercury [e.g., 2-6]. These studies included more detailed layering and temperature-dependent thermophysical properties.

We have extended the analyses of previous work in two ways: 1) An up to date thermal model is used to interpret the relatively high spatial resolution IRR measurements across a wide range of longitudes and local times. To date, the comparison of recent thermal models to measurements has been limited, relying only on limited telescopic microwave emission measurements [2,4,5], or focusing entirely on model-based results to better understand the thermal environment in Mercurian polar regions [3,6]. 2) With the more recent temperature data and associated thermal modeling of the Moon [e.g., 7,8] we are able to make detailed comparisons using the Moon as a framework to better understand and identify similarities and differences in their thermophysical properties.

Surface temperatures were modeled using a 1-dimensional heat diffusion model. The model incorporates properties such as temperature dependent thermal conductivity and heat capacity and solar incidence angle dependent hemispherical albedo. Vertical layering in the model has customizable density, heat capacity, and thermal conductivity of individual layers. The model provides predicted surface and subsurface temperatures for any given input location and time, and can be applied to each Mariner 10 IRR measurement.

Data Processing: The Mariner 10 radiometer dataset consists of brightness temperature measurements at ~1200 unique locations and was retrieved from NASA's Space Science Data Coordinated Archive (NSSDCA).

In order to convert the observed brightness temperature to surface kinetic temperatures, knowledge of the emissivity of the surface and its angular dependence is needed. We adjusted the surface emissivity based on the emission angle of the observation using lunar emission angle-dependent emissivity derived from Diviner data [9]. Our radiance and brightness temperature values closely match example radiance values and brightness temperatures listed in [10].

Results: We modeled surface temperatures to compare them to the retrieved surface temperatures along the IRR measurement transect. There is overlap between the forward-looking and aft-looking observations between ~70–90°E, acquired at different emission angles. After correction for emission angle-dependent emissivity, the temperatures between the two sets of observations match within 1K (Figure 1). NEΔT for IRR at 100K is 0.21K and the instrument used full-aperture space and reference views to produce high quality, well-calibrated measurements.

We focus on the 45 μm channel transect (Figure 1) covering much of the mercurian night from ~10–165°E, and ~10°S–20°N. The derived surface temperatures range from ~100–130K, with local variations of ~5–10K. There are additional observations covering the early morning with both the 11 and 45 μm channels. Although they show useful information regarding surface roughness (e.g., [1]), they are not particularly sensitive to differences in thermophysical properties and are not shown here.

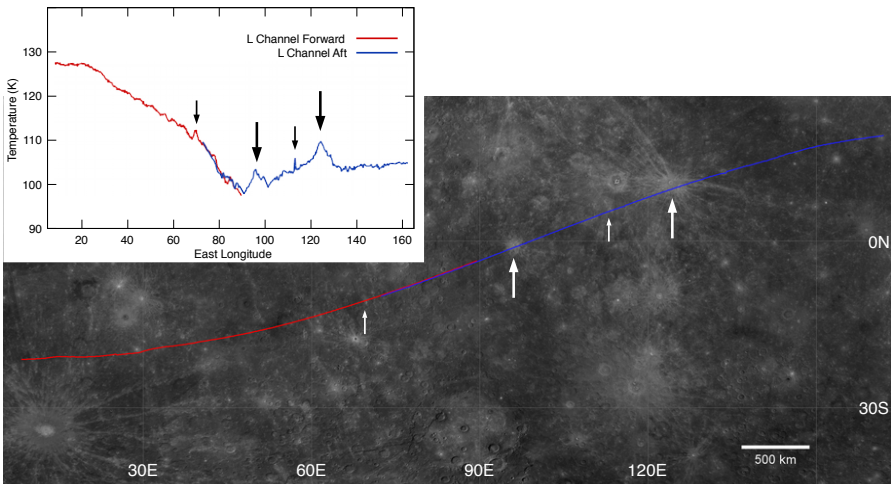

Figure 1: Mariner 10 IRR derived surface temperature transect. The two colors represent the forward (red) and aft (blue) facing measurements. Arrows denote regions of elevated nighttime temperature, likely indicating rockier surfaces that coincide with relatively young impact craters.

Initial test model results using vertically homogeneous properties show consistently low thermal inertia values, similar to previous results (Figure 2; [1]). Most surfaces have TI_{273} values of less than 50 J m^{-2} $s^{-½}$ K^{-1} (because of temperature dependent thermal conductivity and heat capacity, we report thermal inertia referenced to a single temperature – 273K – similar to [8]). The apparent thermal inertia is higher further east and later in the night. Although it is possible that the surface properties show a global-scale longitudinal gradient, this behavior is also consistent with a layered surface that has higher conductivity and density at depth, similar to the lunar environment [7] and consistent with previous measurements [e.g., 2].

The use of a layered model using the h-parameter of [8] produces a much more consistent fit to the measured temperatures across the wide range of longitudes and local times (Figure 2). The h-parameter is the e-folding depth that dictates the change from the thermophysical properties at the surface and at depth [7,8]. In the example shown, the density and thermal conductivity profiles resulted in TI_{273} values of 19 and 71 J m^{-2} $s^{-½}$ K^{-1}at the surface and depth respectively. This is slightly lower than that used for the Moon, which used TI_{273} values of 19 and 91 J m^{-2} $s^{-½}$ K^{-1} [7]. Using these values, a value of 0.09 m for h closely matches the temperatures across most of the transect, with several clear exceptions. This is slightly higher than typical lunar h-parameter values of 0.06 m [7,8].

Discussion: The derived mercurian layered model parameters bear a strong resemblance to typical lunar surfaces, characterized by extremely low thermal inertia values that are distinctly layered. The ability to fit the temperatures across a wide swath of the planet using a single set of thermophysical parameters also suggests that Mercury has large regions with relatively uniform thermophysical properties.

There are notable departures from this uniformity. For example, elevated temperatures are present near 10°N, 125°E that coincide with an immature crater. This is likely due to larger clast sizes present in relatively young ejecta that have not yet broken down in the space weathering environment [e.g., 11–13]. By contrast, longitudes from ~80–95°E show temperatures ~5K lower than the model results, indicating fewer rocks or more loosely packed material in the upper 10's of cm depth [e.g., 8,14]. These lower temperature surfaces may have similarities to lunar "cold spots" [14] or pyroclastic deposits [8].

The observations of Mercury and the Moon provide evidence for similarities between the surfaces of these two bodies. Variations in the regolith and its structure are likely determined by a variety of factors. For example, seismic events and overburden could act to compress and increase the bulk density of the regolith, while micrometeorite impacts disrupt the regolith and cause a lowering of the the bulk density. The Mariner 10 IRR data is limited in spatial scope but comparison to more recent observations of the lunar surface may provide additional insight into the regolith and its formation processes on Mercury.

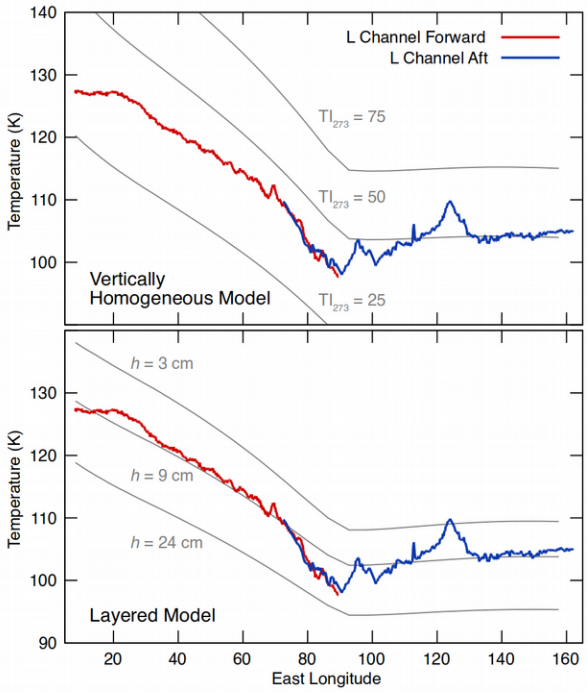

Figure 2: Comparison of Mariner 10 IRR derived surface temperatures with vertically homogeneous (top) and layered (bottom) thermal models. The unlayered model shows low TI_{273} values, typically <50 J m^{-2} $s^{-½}$ K^{-1} that generally increases later during the night. The layered model provides a more consistent fit across a wide range of longitudes and local times.

References: [1] Chase, S.C., et al., (1976) *Icarus*, *28*, 565 [2] Mitchell, D.L. and I. de Pater (1994) *Icarus*, *110*, 2 [3] Vasavada, A.R., D.A. Paige, S.E. Wood, (1999) *Icarus*, *141*, 179 [4] Hale, A.S. and B.W. Hapke (2002) *Icarus*, *156*, 318 [5] Yan, N. et al. (2006) *Adv. Space Res.*, *38*, 583 [6] Paige, D.A., et al. (2013) *Science*, *339*, 300 [7] Vasavada, A.R., et al. (2012) *JGR*, 10.1029/2011JE003987 [8] Hayne, P.O., et al. (2017) *JGR*, 10.1002/2017JE005387 [9] Bandfield, J.L., et al. (2015) Icarus, *248*, 357 [10] Clarke, T.C. (1975) Tech. Memo. 33-719, *JPL* [11] Mendell, W.W., and F.J. Low (1974) *Moon*, *9*, 97 [12] Bandfield, J.L., et al. (2011) *JGR*, 10.1029/2011JE003866 [13] Ghent, R.R., et al. (2013) Geology, *42*, 1059 [14] Bandfield, J.L., et al. (2014) *Icarus*, *231*, 221